

# Iron-Embedded Porous Carbon Nanofibers as Pt Electrocatalyst Supports for Direct Methanol Fuel Cells

Dong-Yo Shin, Geon-Hyoung An, and Hyo-Jin Ahn\*

*Department of Materials Science and Engineering, Seoul National University of Science and Technology, Seoul 139-743, South Korea*

Pt electrocatalysts well-dispersed on iron (Fe)-embedded porous carbon nanofiber (CNF) supports were synthesized using electrospinning and a reduction method for improved methanol electro-oxidation. To study the effects of the amount of Fe embedded in the porous CNF supports, we used three different amounts of Fe precursor: 4 wt% (sample A), 8 wt% (sample B), and 12 wt% (sample C). Among them, sample B exhibited the highest anodic current density of 619.0 mA/mg<sub>Pt</sub> and excellent electrocatalytic stability compared to commercial Pt/C and Pt/CNFs. The enhanced methanol electro-oxidation performance can be explained by the combined effects of increased active area between the Pt electrocatalysts and the electrolyte due to well-dispersed Pt electrocatalysts on porous CNF supports, and the improved electrical conductivity of the supports due to the efficient electron transfer by Fe nanoparticles embedded within porous CNFs.

**Keywords:** Methanol Electro-Oxidation, Platinum Electrocatalysts, Porous Carbon Nanofibers, Electrospinning, Iron Nanoparticles.

## 1. INTRODUCTION

With dramatic industry development, resource depletion and environmental pollution are becoming serious problems. As a potential solution to these problems, direct methanol fuel cells (DMFCs), which convert chemical energy of methanol fuel to electric energy, have received considerable attention owing to their advantages of high energy density (6.1 kWh/kg), high energy conversion efficiency (>80%), low operating temperature (room temperature-to 120 °C), and simple configuration.<sup>1-3</sup> In general, a DMFC is composed of a cathode, an anode, a membrane, and an electrolyte. At the anode, the methanol electro-oxidation under electrocatalysts is the key factor for achieving high performance DMFCs.<sup>4,5</sup> However, the use of Pt electrocatalysts at the anode has serious disadvantages such as high cost, low active area due to Pt agglomeration, and CO poisoning owing to the absorption of carbonaceous species (CO, COOH, and CHO) on the Pt surface.<sup>6,7</sup> To overcome these problems, many strategies have been studied, such as nanosized Pt electrocatalysts, Pt-metal alloys, control of catalyst crystal plane, and use of catalyst supports.<sup>8-11</sup> Among these strategies, the introduction of catalyst supports using

carbon-based materials, metal oxide-based materials, or conducting polymers are one of the most promising techniques to minimize Pt loading, increase active area of the catalyts, and enhance the electrocatalytic stability in DMFCs.<sup>12,13</sup> Among carbon-based materials, carbon nanofibers (CNFs) have been studied because it has the advantages of high specific surface area (448 m<sup>2</sup>/g), low electrical resistivity (1.7 × 10<sup>3</sup> S/m), relatively low cost, and thermal/chemical stability.<sup>14</sup> For example, Nakagawa et al. fabricated PtRu alloy decorated on CNFs with titanium dioxide for methanol electro-oxidation using an electrospinning method. The authors reported a current density of 202 mA/g, 1.61 times higher than that of commercial PtRu/C (Tanaka Kikinzoku Kogyo K. K.).<sup>15</sup> Jin et al. synthesized PtRu alloy coated CNFs using electrospinning and a reduction method, and reported a current density of 63.1 mA/mg<sub>Pt</sub>, 1.59 times higher than that of conventional Pt/CNFs.<sup>16</sup> Zhao et al. synthesized Pt catalysts-decorated porous CNFs using a self-assembly method, reported a current density of 69.6 mA/cm<sup>2</sup>, 1.72 times higher than that of commercial Pt/C (E-TEK).<sup>17</sup> Nevertheless, the introduction of Fe-embedded porous CNF, which have porous structure and high electrical conductivity, as supports for well-dispersed Pt electrocatalysts, has not been reported.

\*Author to whom correspondence should be addressed.

In this research, we synthesized well-dispersed Pt electrocatalysts on Fe-embedded porous CNF supports using electrospinning and a reduction method, and demonstrated their use as anode materials for improved methanol electro-oxidation in DMFCs.

## 2. EXPERIMENTAL DETAILS

Fe-embedded porous carbon nanofibers (CNFs) were fabricated by electrospinning and Pt was added onto the supports using a reduction method. First, to synthesize Fe-embedded porous CNFs, 10 wt% polyacrylonitrile (PAN, Mw = 150,000 g/mol, Aldrich) and iron(II) phthalocyanine ( $\text{FeC}_{32}\text{H}_{16}\text{N}_8$ , Mw = 568.37 g/mol, Aldrich) were dissolved in *N,N*-dimethylformamide (DMF, Aldrich) for 10 h. To control the morphology of Fe-embedded porous CNFs, the iron phthalocyanine precursor was controlled by three different weight ratios of 4 wt%, 8 wt%, and 12 wt% in this process. For electrospinning, the above solution was placed in a 12 ml syringe equipped with a 23-gauge needle. The voltage and feeding rate were maintained at 17 kV and 0.03 ml h<sup>-1</sup>, respectively. The distance between the needle and the collector was maintained at 15 cm under 10% humidity at room temperature. The prepared nanofibers were stabilized at 280 °C for 2 h in air and carbonized at 800 °C for 2 h under nitrogen atmosphere (99.999%). Subsequently, in order to obtain the porous CNF supports, H<sub>2</sub>-treatment was performed using a mixed gas (N<sub>2</sub>:H<sub>2</sub> = 90%:10%) at 800 °C for 5 h. This H<sub>2</sub> treatment caused the agglomeration of Fe nanoparticles outside the porous CNFs. Then, the agglomerated Fe particles were removed by acid treatment using a mixed solution of hydrogen fluoride (HF, 52%) and nitric acid (HNO<sub>3</sub>, 66%). In this manner, Fe-embedded porous CNFs were synthesized successfully. To synthesize Pt electrocatalysts on Fe-embedded porous CNFs, 40 wt% Pt was reduced onto the supports with H<sub>2</sub>PtCl<sub>6</sub> · xH<sub>2</sub>O (Aldrich). The Fe-embedded porous CNFs were dispersed in DI-water and then H<sub>2</sub>PtCl<sub>6</sub> · xH<sub>2</sub>O was added to the suspension with a concentration of 1.12 mM. Then, concentrated NaBH<sub>4</sub> solution (100 mg/mL) was added as the reducing agent. The resultant samples were washed several times with DI-water and freeze-dried at -50 °C using liquid nitrogen. As a result, we obtained 40 wt% Pt electrocatalysts on Fe-embedded porous CNFs previously synthesized with 4 wt%, 8 wt%, and 12 wt% Fe precursor (herein designated as sample A, B, and C respectively).

Commercial Pt/C catalysts (40 wt% Pt on Vulcan carbon, E-TEK, now a division of Industrie De Nora S.P.A., Italy) were used for comparison purposes. In addition, to compare the effects of Fe-embedded porous CNFs, Pt catalysts decorated on conventional CNFs (hereafter referred to as Pt/CNFs) were also prepared by the above-mentioned method.

The morphologies and structures of the samples were determined by field-emission scanning electron

microscopy (FESEM; Hitachi S-4800) and transmission electron microscopy (TEM; Tecnai G<sup>2</sup>, KBSI Gwangju Center). Electrical conductivity of Pt/CNFs and sample B was measured using a Hall effect measurement system (Ecopia, HMS-3000). To prepare for electrical conductivity measurement, a slurry consisting of 80 wt% of the sample, and 20 wt% poly(vinylidene difluoride) (PVDF) as a binder in *N*-methyl-2-pyrrolidinone (NMP, 99.5%) was coated on paper insulator, and the resultant electrodes were dried at 80 °C for 10 h. The crystal structure and chemical bonding states were observed using X-ray diffractometry (XRD, Rigaku D/MAX2500 V) and X-ray photoelectron spectroscopy (XPS, ESCALAB 250 equipped with an Al K<sub>α</sub> X-ray source). Electrochemical performance measurements were carried out with a potentiostat/galvanostat (PGST302N, Eco Chemie) using a glassy carbon (0.07 cm<sup>2</sup>) working electrode, a Pt wire counter electrode, and a Ag/AgCl (saturated KCl) reference electrode. Electrocatalyst ink was prepared for the measurement by dispersing 10 mg of a sample by ultrasonication and stirrer in 0.9 ml of 2-propanol and 0.1 ml of DI-water containing 5 wt% Nafion. The prepared ink was carefully dropped onto the glassy carbon electrode to obtain a Pt catalyst loading of around 30 μg/cm<sup>2</sup> and dried at 70 °C. The methanol electro-oxidation performance was measured by cyclic voltammetry (CV) in a 2 M CH<sub>3</sub>OH and 0.5 M H<sub>2</sub>SO<sub>4</sub> electrolyte between -0.2 and 1.0 V (vs. Ag/AgCl) at a scan rate of 50 mV/s. The electrocatalytic stability was examined by chronoamperometry (CA) in a mixture of 2 M CH<sub>3</sub>OH and 0.5 M H<sub>2</sub>SO<sub>4</sub> at a constant voltage of 0.5 V for 2000 s.

## 3. RESULTS AND DISCUSSION

Figure 1 shows a schematic illustration of the synthesis steps for well-dispersed Pt electrocatalysts on Fe-embedded porous CNF supports using an electrospinning

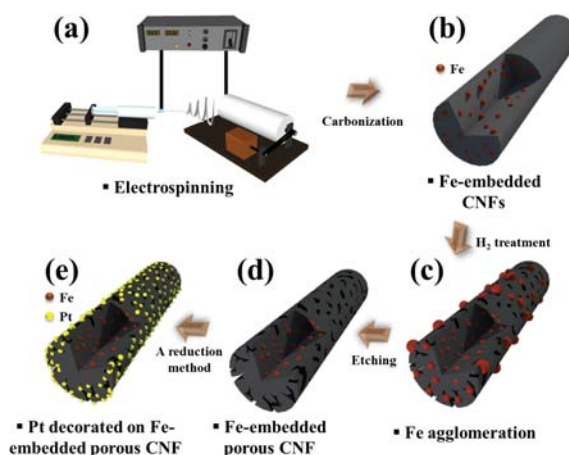


**Figure 1.** Schematic illustration of the synthesis steps for high dispersion of Pt electrocatalysts on Fe-embedded porous CNF supports.

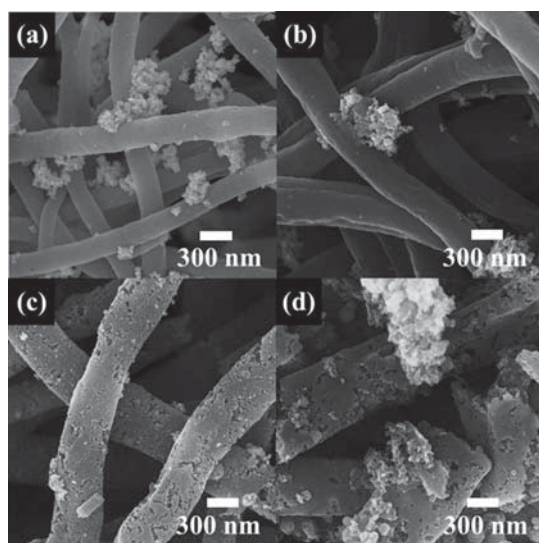


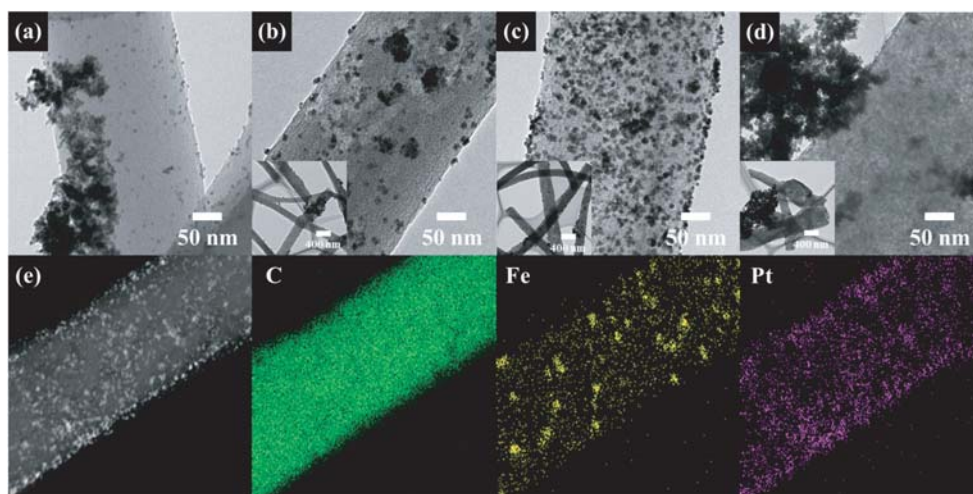
**Figure 2.** FESEM images obtained from (a) Pt/CNFs, (b) sample A, (c) sample B, and (d) sample C.

method followed by a reduction method. First, the as-spun nanofibers consisting of PAN and Fe precursor were synthesized by electrospinning (Fig. 1(a)). Then, Fe nanoparticles were embedded in CNFs by carbonization (Fig. 1(b)). To synthesize the porous CNF supports containing Fe nanoparticles,  $H_2$ -treatment was performed. Pores of supports were formed by Fe agglomeration on surface, as shown in Figure 1(c).<sup>18</sup> After  $H_2$ -treatment, the agglomerated Fe particles on surface was removed using an acid treatment (Fig. 1(d)) to maintain the Fe nanoparticles only inside the porous CNF supports. Finally, well-dispersed Pt electrocatalysts on Fe-embedded porous CNF supports were successfully synthesized by a reduction method (Fig. 1(e)). Methanol electro-oxidation performances were

improved by a synergy effect of increased active area between Pt electrocatalysts and electrolyte related to well-dispersed Pt electrocatalysts on supports, and improved electrical conductivity of supports related to efficient electron transfer by embedded Fe nanoparticles.

Figure 2 shows FESEM images of Pt/CNFs, sample A, sample B, and sample C with the average diameters of 265.4 nm, 283.7 nm, 306.9 nm, and 510.4 nm respectively. In terms of morphological properties, Pt/CNFs and sample A (Figs. 2(a and b)) exhibited a smooth CNF surface, while sample B (Fig. 2(c)) exhibited rough surfaces owing to the embedded Fe nanoparticles with pores. However, sample C showed the destruction of CNFs with the significantly larger diameter attributed to the large amount of Fe nanoparticles. In addition, Pt/CNFs and sample A indicated the agglomerated Pt electrocatalysts sparsely because of the smooth surface and low amount of pores respectively. In the case of sample B, the Pt electrocatalysts were well dispersed, and therefore no agglomerate was observed. This means that sample B had high surface roughness due to high porosity.<sup>19</sup> In contrast, sample C showed high agglomeration of Pt electrocatalysts owing to the destruction of CNFs. In methanol electro-oxidation, the morphology of these well-dispersed Pt electrocatalysts on Fe-embedded porous CNFs is the key factor for the improvement of electrocatalytic activity by increasing the active area between Pt electrocatalysts and electrolyte.

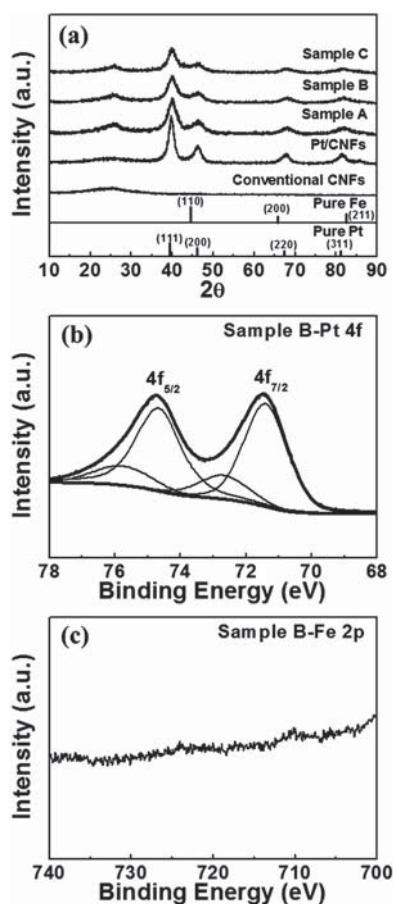
To further investigate the morphological properties of all samples, TEM measurements were performed. Figure 3 shows the TEM data obtained for the Pt/CNFs, sample A, sample B, and sample C. Pt/CNFs (Fig. 3(a)) showed large agglomerated Pt electrocatalysts as the dark contrast areas. Fe nanoparticles with the size of 12.8 nm–16.1 nm embedded in porous CNFs were observed in samples A, B, and C. The embedment increased electrical conductivity of the porous CNF supports was increased because



**Figure 3.** TEM images of (a) Pt/CNFs, (b) sample A, (c) sample B, and (d) sample C. (e) TEM-EDS mapping data of sample B.

of Fe nanoparticles embedded within porous CNF supports. Especially, the electrical conductivity of sample B was measured at 15.59 S/cm, higher than that of Pt/CNFs (1.56 S/cm). Sample A (Fig. 3(b)) exhibited agglomerated Pt electrocatalysts sparsely distributed on Fe embedded porous CNF surface. In the case of sample B (Fig. 3(c)), the Pt electrocatalysts showed excellent dispersion on Fe embedded porous CNF surface owing to the high roughness and porosity at the surface. However, sample C exhibited serious agglomeration of Pt electrocatalysts due to the large size of CNFs caused by the excessive addition of Fe precursor (12 wt%). Therefore, sample B, having excellent dispersion of Pt electrocatalysts, was favorable for improved methanol electro-oxidation owing to the increased number of active sites of Pt electrocatalysts. This results mean that well dispersion of nanosized electrocatalysts is a key factor for enhancing electrocatalytic activity and stability of DMFCs.<sup>20,21</sup> To confirm the dispersion of Pt electrocatalysts and the embedment of Fe nanoparticles throughout the supports for sample B, TEM-energy dispersive spectroscopy (TEM-EDS) mapping analysis was performed, as shown in Figure 3(e). Based on the SEM, TEM, and TEM-EDS mapping results, we concluded that the embedment of Fe nanoparticles can affect the roughness of the CNF supports, and therefore the dispersion of Pt electrocatalysts. There was an optimum amount of added Fe nanoparticles to achieve the best dispersion.

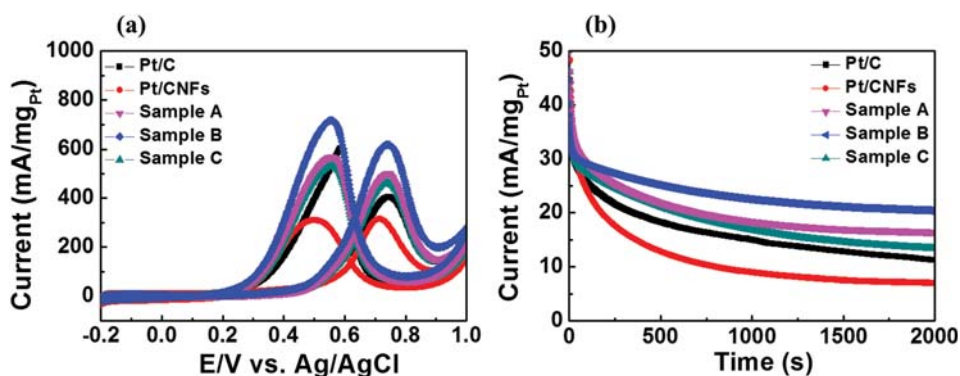
Figure 4(a) shows XRD data for conventional CNFs, Pt/CNFs, sample A, sample B, and sample C. A broad diffraction peak was observed for all samples at  $2\theta$  of approximately  $= 25^\circ$ , corresponding to the (200) layer of graphite. The main diffraction peaks of Pt/CNFs, sample A, sample B, and sample C were observed at  $39.7^\circ$ ,  $46.2^\circ$ ,  $67.4^\circ$ , and  $81.3^\circ$ , corresponding to the (111), (200), (220), and (311) planes of Pt respectively. These planes represented the face-centered cubic structure with the space group  $Fm\bar{3}m[225]$  of Pt (JCPDS card No. 04-0802). Additional peaks were observed for the Fe-embedded porous CNF supports at  $44.7^\circ$ ,  $65.0^\circ$ , and  $82.4^\circ$ . These peaks correspond to the (110), (200), and (211) planes of the body-centered cubic structure with the space group  $Im\bar{3}m[229]$  of Fe (JCPDS card No. 87-0721). In addition, XRD data of samples A, B, and C in the  $40^\circ$ – $47^\circ$  range showed that the peak intensity of the Fe (110) plane increased with increasing amount of Fe nanoparticles in porous CNFs. Figures 4(b) and (c) exhibit XPS spectra of the Pt  $4f$  and Fe  $2p$  core levels for sample B. The binding energies of the Pt  $4f$  and Fe  $2p$  spectra were calibrated to the binding energy of  $C 1s$  for adventitious carbon at 284.5 eV. The Pt  $4f$  spectrum consisting of the Pt  $4f_{7/2}$  and  $4f_{5/2}$  doublet at 71.3 eV and 74.6 eV respectively corresponded to Pt metallic state. The energy separation between the Pt  $4f_{7/2}$  and  $4f_{5/2}$  peaks was 3.3 eV, and their ratio agreed with the theoretical value of 4:3.<sup>22</sup> Another



**Figure 4.** (a) XRD data of conventional CNFs, Pt/CNFs, sample A, sample B, and sample C. (b) XPS spectra of Pt  $4f$  and Fe  $2p$  core levels of sample B.

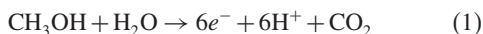
small doublet at 72.3 eV and 75.4 eV corresponding to Pt(II) oxidation state such as PtO and Pt(OH)<sub>2</sub> was also observed.<sup>22</sup> This result means that the Pt synthesized on Fe-embedded porous CNFs surface existed mainly in the metallic state, which is consistent with the XRD results. Fe  $2p$  XPS spectral peaks were not detected because of limited resolution of X-ray (1–10 nm). Based on the FESEM, TEM, XRD, and XPS results, it can be seen that well-dispersed Pt electrocatalysts on Fe-embedded porous CNFs were successfully synthesized.

Figure 5(a) shows the cyclic voltammetry (CV) curves of methanol electro-oxidation using commercial Pt/C, Pt/CNFs, sample A, sample B, and sample C. CV was performed at the scan rate of 50 mV/s between  $-0.2$  V and 1.0 V (vs. Ag/AgCl) using a mixed solution of 0.5 M H<sub>2</sub>SO<sub>4</sub> and 2 M CH<sub>3</sub>OH. In general, the CV curves of methanol electro-oxidation showed two peaks of the forward and backward sweeps corresponding respectively to the main anodic current density and that involved the intermediate species such as CH<sub>2</sub>OH, HCOOH, CHO, and



**Figure 5.** (a) Cyclic voltammograms of commercial Pt/C, Pt/CNF, samples A, sample B, and sample C in a mixed solution of 0.5 M H<sub>2</sub>SO<sub>4</sub> and 2 M CH<sub>3</sub>OH at scan rate of 50 mV/s. (b) Chronoamperometry of commercial Pt/C, Pt/CNFs, samples A, sample B, and sample C in a mixed solution of 0.5 M H<sub>2</sub>SO<sub>4</sub> and 2 M CH<sub>3</sub>OH at 0.5 V.

CO.<sup>23,24</sup> The methanol electro-oxidation at the anode produces 6 protons, 6 electrons, and carbon dioxide.



The methanol electro-oxidation efficiency is directly related to the intensity of the CV forward peak. High intensity means that a large amount of electrons has been produced by methanol electro-oxidation. The anodic current densities of commercial Pt/C, Pt/CNFs, sample A, sample B, and sample C were 405.1, 315.0, 502.7, 619.0, and 455.9 mA/mg<sub>Pt</sub>, respectively. As can be seen, sample B exhibits the highest anodic current density among all samples because of well-dispersed Pt electrocatalysts on the supports related to high active area of Pt electrocatalysts, and increased electrical conductivity related to efficient electron transfer by optimum amount of Fe nanoparticles within porous CNF supports. These results showed 1.53, 1.97, 1.23, and 1.36 times higher compared to the commercial Pt/C, Pt/CNFs, sample A, and sample C, respectively. To further investigate the electrocatalytic stability of all samples, chronoamperometry (CA) measurements (Fig. 5(b)) were carried out. A current decay occurred during the initial stage for all samples owing to the adsorption of interfering species such as CH<sub>3</sub>OH, CHO, and SO<sub>4</sub><sup>2-</sup> anions onto the Pt electrocatalyst surface.<sup>25</sup> The adsorption reduces the active area between the electrocatalysts and the electrolyte. Nevertheless, sample B exhibited the highest anodic current density and excellent electrocatalytic stability compared to other samples. The high methanol electro-oxidation performance of sample B can be explained by two major reasons. One is that, the well-dispersed Pt electrocatalysts on Fe-embedded porous CNFs provided an increased active area between the Pt electrocatalysts and the electrolyte. The other is that the optimum amount (8 wt%) of Fe nanoparticles embedded in porous CNFs improved electrical conductivity of the supports. These results suggest that Fe-embedded porous CNFs are promising supports for efficient DMFCs.

## 4. CONCLUSION

Well-dispersed Pt electrocatalysts on Fe-embedded porous CNF supports were successfully synthesized using electrospinning and a reduction method. To study the effects of the amount of embedded Fe, the added Fe precursor contents were set at 4 wt% (sample A), 8 wt% (sample B), and 12 wt% (sample C). Among them, sample B showed the highest anodic current density (619.0 mA/mg<sub>Pt</sub>) and excellent electrocatalytic stability compared to all other samples including commercial Pt/C and Pt/CNFs. The improved methanol electro-oxidation performance can be attributed to two main effects:

- (I) the increased active area between the Pt electrocatalyst and the electrolyte due to the good dispersion of the Pt electrocatalysts on the supports;
- (II) the improved electrical conductivity due to the Fe nanoparticles embedded within porous CNFs.

**Acknowledgments:** This research was supported by Basic Science Research Program through the National Research Foundation of Korea (NRF) funded by the Ministry of Science, ICT and Future Planning (NRF-2015R1A1A1A05001252).

## References and Notes

1. Z. Yang and N. Nakashima, *Sci. Rep.* 5, 12236 (2015).
2. Y. Feng, F. Ye, H. Liu, and J. Yang, *Sci. Rep.* 5, 16219 (2015).
3. P. L. Antonucci, A. S. Arico, P. Creti, E. Ramunni, and V. Antonucci, *Solid State Ionics* 125, 431 (1999).
4. E. S. Steigerwalt, G. A. Deluga, and C. M. Lukehart, *J. Phys. Chem. B* 106, 760 (2002).
5. A. S. Arico, P. Creti, H. Kim, R. Mantegna, N. Giordano, and V. Antonucci, *J. Electrochem. Soc.* 143, 3950 (1996).
6. T. Seiler, E. R. Savinova, K. A. Friedrich, and U. Stimming, *Electrochim. Acta* 49, 3927 (2004).
7. R. Manoharan and J. Prabhuram, *J. Power Sources* 96, 220 (2001).
8. K. Yamamoto, T. Lmaoka, W.-J. Chun, O. Enoki, H. Katoh, M. Takenaga, and A. Sonoi, *Nat. Chem.* 1, 397 (2009).
9. M. Oezaslan, F. Hasche, and P. Strasser, *J. Phys. Chem. Lett.* 4, 3273 (2013).

10. V. R. Stamenkovic, B. Fowler, B. S. Mun, G. Wang, P. N. Ross, C. A. Lucas, and N. M. Markovi, *Science* 315, 493 (2007).
11. J. Greeley and M. Mavrikakis, *Nat. Mater.* 3, 810 (2004).
12. Y. Mu, H. Liang, J. Hu, L. Jiang, and L. Wan, *J. Phys. Chem. B* 109, 22212 (2005).
13. L. Liu, C. Pu, R. Viswanathan, Q. Fan, R. Liu, and E. S. Smotkin, *Electrochim. Acta* 43, 3657 (1998).
14. G.-H. An and H.-J. Ahn, *Electrochem. Solid State Lett.* 3, M29 (2014).
15. N. Nakagawa, Y. Ito, T. Tsujiguchi, and H. Ishitobi, *J. Power Sources* 248, 330 (2014).
16. X. Jin, B. He, J. Miao, J. Yuan, Q. Zhang, and L. Niu, *Carbon* 50, 3083 (2012).
17. G. Zhao, J. He, C. Zhang, J. Zhon, X. Chen, and T. Wang, *J. Phys. Chem. C* 112, 1028 (2008).
18. G.-H. An, E.-H. Lee, and H.-J. Ahn, *J. Alloys Compd.* 682, 746 (2016).
19. F. Su, Z. Tian, C. K. Poh, Z. Wang, S. H. Lim, Z. Liu, and J. Lin, *Chem. Mater.* 22, 832 (2010).
20. J.-D. Qiu, G.-C. Wang, R.-P. Liang, X.-H. Xia, and H.-W. Yu, *J. Phys. Chem. C* 115, 15639 (2011).
21. Z. Liu, X. Y. Ling, J. Y. Lee, X. Su, and L. M. Gan, *J. Mater. Chem.* 13, 3049 (2003).
22. F. Sen and G. Gokagac, *J. Phys. Chem. C* 111, 5715 (2007).
23. G.-H. An, E.-H. Lee, and H.-J. Ahn, *Phys. Chem. Chem. Phys.* 18, 14859 (2016).
24. J. W. Guo, T. S. Zhao, J. Prabhuram, R. Chen, and C. W. Wong, *Electrochim. Acta* 51, 754 (2005).
25. Z. Ji, X. Shen, G. Zhu, K. Chen, G. Fu, and L. Tong, *J. Electroanal. Chem.* 682, 95 (2012).

Received: 16 August 2016. Accepted: 13 January 2017.